Threshold displacement and interstitial-atom formation energies in Ni_3Al

A. Caro[a] and M. Victoria
Paul Scherrer Institute, CH-5232 Villingen, Switzerland

R. S. Averback
Department of Materials Science and Engineering, University of Illinois at Urbana–Champaign, Urbana, Illinois 61801

(Received 7 December 1989; accepted 20 March 1990)

Threshold displacement energies for atomic displacements along ⟨110⟩, ⟨100⟩, and ⟨111⟩ directions, and formation enthalpies of several symmetric interstitial atom configurations were calculated for Ni_3Al by computer simulation using "embedded atom method" potentials. The Ni–Ni (100) dumbbell in the plane containing only Ni atoms has the lowest interstitial-atom enthalpy although the enthalpies of other configurations are similar. Interstitial configurations involving Al atoms all have much higher enthalpies. The anisotropy of the threshold energies in Ni_3Al is similar to pure metals and no significant difference in threshold energy was observed for ⟨110⟩ replacement chains in rows containing all Ni atoms or alternating Ni–Al atoms. Various metastable interstitial atom configurations were observed, including crowd-ions. In addition, the spontaneous recombination volume for some configurations can be much smaller than in pure metals. The consequences of these results for radiation induced segregation and amorphization are discussed.

I. INTRODUCTION

Computer simulation has been found to be a powerful method for investigating the mechanisms of defect production[1,2] and for calculating point defect properties.[3] Although these studies have been performed mostly on pure metals, advances in computing capabilities and the development of realistic, yet tractable, interatomic potentials now make it possible to study a number of alloy systems as well.[4] We have begun such studies and present here calculations of the threshold energy for Frenkel pair production and the formation enthalpy of interstitial-type defects in the ordered alloy, Ni_3Al. Ni_3Al is of interest for several reasons. First, Ni_3Al provides an interesting ordered structure ($L1_2$) for threshold energy investigations since along some close packed directions ⟨110⟩ the atoms are all Ni whereas along others, they are alternating Ni and Al. The effect of the mass mismatch for the propagation of RCSs is not known although it was considered briefly by Vineyard and co-workers years ago.[5] Replacement sequences along other close packed directions, ⟨100⟩, contain pure Al and pure Ni chains. The point defect properties in Ni_3Al are also of interest since the high ordering energy may influence point defect configurations, the spontaneous recombination volume, and point defect diffusion mechanisms. Finally, reliable "embedded atom method" (EAM) potentials are available for the Ni–Al system.[6] Vacancy properties in Ni_3Al were studied previously,[6] so we restrict our investigation here to the interstitial-atom properties. One of the motivations for undertaking this investigation was the finding that radiation-induced segregation[7] in this alloy is very small. This result is interesting, since radiation-induced segregation has been observed in terminal-phase (γ) solutions of Ni–Al alloys,[8] suggesting that atomic ordering plays an important role in segregation effects. We will show that this is indeed the case.

II. RESULTS

Numerical simulations were made using code DYN52,[9] with the input function for the Ni–Al alloys reported in Ref. 5. A cubic cluster containing 11^3 elementary cells, or 5324 atoms, with fixed, periodic boundary conditions is used for the displacement events, while constant pressure is used for static relaxations.

A. Interstitial atom formation enthalpies

We begin our investigation of the properties of Ni_3Al under irradiation with calculations of the formation enthalpies of interstitial type point defects. Vacancy and anti-site defect enthalpies were reported in Ref. 6 but are included in our Table I for convenience. The stacking of the $L1_2$ structure along the ⟨100⟩ direction is ABAB. . , where A is a plane containing 50% of Ni and

[a]Fellow of the Consejo Nacional de Investigaciones Cientificas y Tecnicas Argentina.

TABLE I. Formation energies and volumes of the relevant intrinsic point defects in Ni_3Al.

Type of defect		ΔE_f (eV)	ΔV_f (Ω_0)
Al	Vacancy	1.91	0.83
Ni	Vacancy	1.47	0.96
Al	Anti-site	0.54	0.35
Ni	Anti-site	0.58	0.35
Dumbbell	Ni–Ni (B)	3.63	0.67
Dumbbell	Ni–Ni (A)	4.67	0.85
Dumbbell	Al–Al (A)	6.22	1.38
Dumbbell	Ni–Al* (B)	4.45	1.00
Dumbbell	Ni–Al* (A)	6.21	1.59
Dumbbell	Ni*–Al (A)	4.89	1.11
Octahedral	Ni (A)	4.97	1.11
Octahedral	Ni (B)	3.77	0.47
Octahedral	Al (A)	6.53	1.53
Octahedral	Al (B)	4.54	0.87
Crowd-ion	Ni (A)	5.14	1.08
Crowd-ion	Ni (B)	3.74	2.27
Crowd-ion	Al (A)	6.19	1.85
Crowd-ion	Al (B)	4.54	0.98

(A) and (B) indicate the type of plane where the defect atom or atoms are located. The symbol (*) indicates the extra atom in the dumbbell. Schematic representations of the defects are shown in Figs. 1 and 2. Ω_0 is the average atomic volume $1/4 \cdot a_0^3$.

50% of Al, and B contains 100% Ni. Besides the two types of vacancies and the two types of anti-site defects in this structure (the latter represented by "a" and "b" in Fig. 1), several types of interstitials are possible. In fact, there are six possible dumbbell configurations, four octahedrals, and four proper crowd-ions. Since some of them are relevant in the displacement events, we have calculated their formation enthalpies.

1. Dumbbells

In the Al sublattice, an extra Al or Ni atom generates a dumbbell which has eight Ni atoms as nearest neighbors (nn), independently of its orientation along any one of the three major crystallographic axes. The neighbor list is different in the Ni sublattice. A Ni atom can belong to an A or to a B plane, depending on the direction of stacking. An additional Al or Ni atom will create a different defect, depending on whether the dumbbell axis lies in an A or B plane. This asymmetry is illustrated in Fig. 2, where it can be seen that the Ni–Al (B) or Ni–Ni (B) dumbbells have eight atoms nn, while the Ni–Al (A) or Ni–Ni (A) dumbbells have four Ni and four Al atoms as nn. Due to the large difference in atomic size between Ni and Al, these configurations have quite different formation enthalpies. The interstitial with lowest enthalpy is the Ni–Ni (B), whereas the highest is the Al–Al (A).

The three possible configurations of an Al interstitial [Figs. 1(c), 2(a), and 2(b)] are unstable with respect to the formation of a Ni anti-site defect plus a Ni–Ni

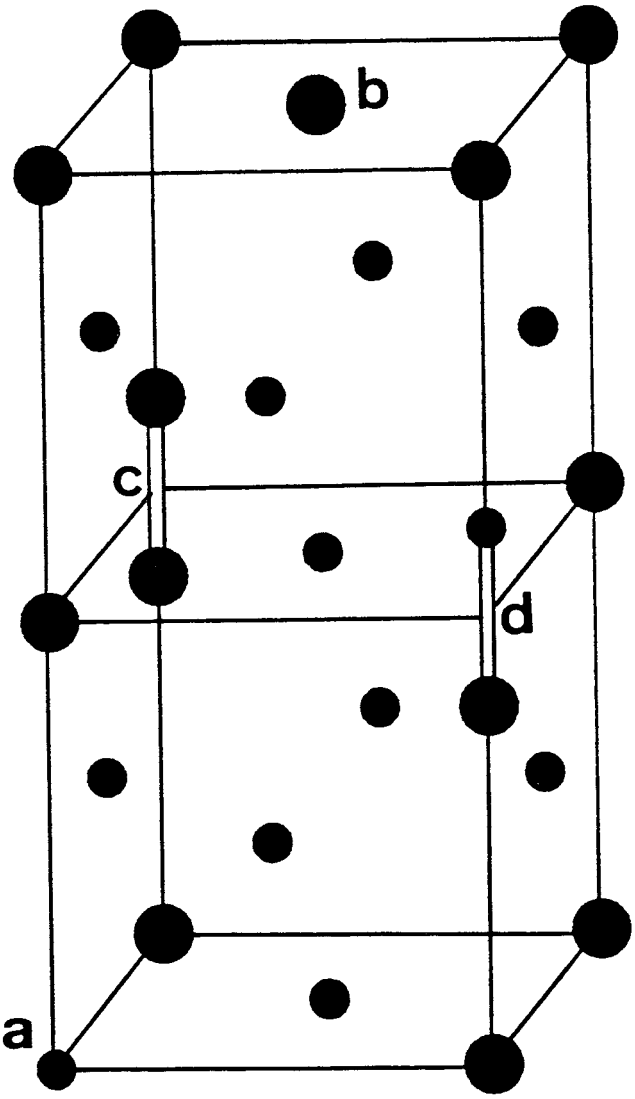

FIG. 1. Schematic representation of the point defects in the $L1_2$ structure. Large (small) circles represent Al (Ni) atoms. (a) Al-anti-site; (b) Ni-anti-site; (c) Al–Al interstitial; and (d) Ni*–Al interstitial, with Ni the extra atom. Cases (c) and (d) are independent of the orientation with respect to the cubic axis.

(B) interstitial; therefore an Al interstitial is immobile since it converts into an anti-site defect. For the three possible configurations of a Ni interstitial, that in the Al sublattice is the most energetic. This, and the Ni–Ni (A), will convert into the Ni–Ni (B). We point out that since interstitial migration involves rotation of the dumbbell axis, the Ni–Ni ⟨100⟩ interstitial can perform three-dimensional migration without changing its nature (that is, the dumbbell axis can remain on a B plane). The Ni–Ni (B), therefore, appears to be the only mobile species in this structure.

2. Octahedrals

Two types of octahedrals are possible. In one case, (A), the interstitial site is contained in the intersection

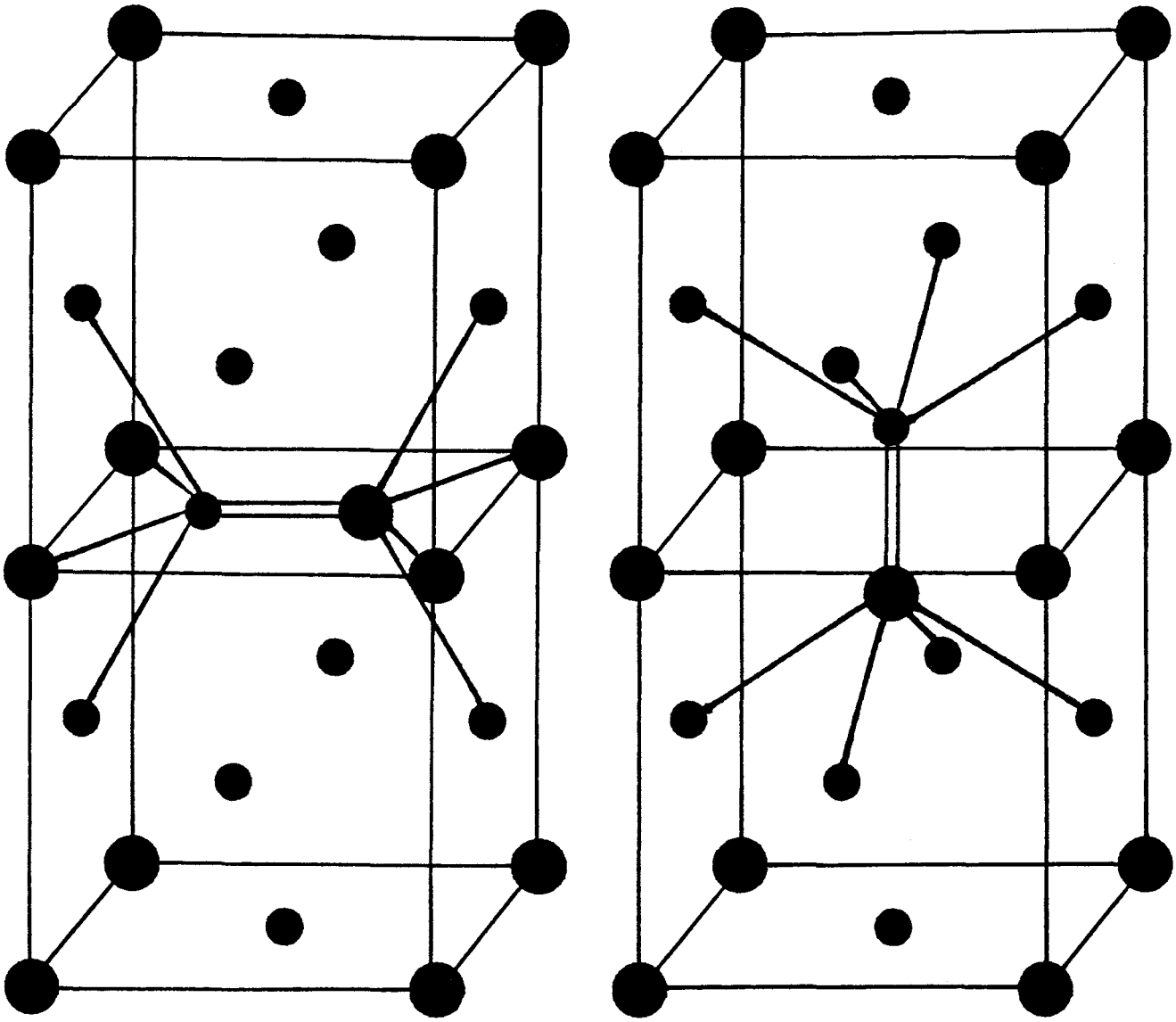

FIG. 2. Schematic representation of the Ni–Al* interstitial with Al the extra atom. (a) (A) plane; in this case four Ni and four Al atoms are nn to the interstitial. (b) (B) plane; in this case eight Ni atoms are nn. Ni–Ni interstitials are similar.

of two A and one B plane. In the other, (B), it is contained in the intersection of three B planes. When these sites are occupied by Al or Ni atoms, four cases appear. As expected from simple size arguments, the Ni (B) has the lowest formation enthalpy among the octahedrals.

3. Crowd-ions

Four crowd-ion configurations in the $L1_2$ structure are determined by whether the defect axis is contained in the A or B plane and on the identity of the extra atom. These "proper" crowd-ions are not the ones which appear in the displacement events shown in the next section. There, the crowd-ions are located at the end of replacement collision sequences, RCSs, and are composed of linear arrays of anti-site defects plus an extra atom. These are complex defects which cannot be classified into any one of the four proper categories.

As usual, the differences in enthalpy between corresponding dumbbell, octahedral, and crowd-ion configurations are small, typically 0.1 to 0.2 eV. Dumbbells, however, are favored.

B. Displacement energies

For each crystallographic direction, replacement collision sequences can propagate along two nonequivalent rows of atoms. The ⟨110⟩ RCS can be contained in an A or B plane. In the first case, Ni atoms collide with

Al atoms and vice versa; in the second case, only Ni atoms participate. Replacements in the ⟨100⟩ direction can propagate on either A or B planes, but they contain only a single type of atom, Al atoms if they cross the center of the cubic cell, and Ni atoms if they cross the center of a cube face.

We have analyzed several possibilities. First we tested the adequacy of the EAM potentials to describe the threshold energy. Table II shows the results of those simulations. The behavior of ⟨110⟩ RCSs in an A plane is similar for Al and Ni primary knock-on atoms (PKAs): the threshold energy is between 20 and 30 eV. It is noteworthy that the empirical functions used in the EAM are not adjusted to threshold energies; therefore, the correct values are to be considered as a somewhat fortuitous coincidence.[10] We find that the displacement energy in the ⟨110⟩ directions on B planes is about the same as on A planes, even though these events involve only Ni atoms, indicating that the mass mismatch for RCSs along ⟨110⟩ B planes is not an important factor in replacement sequences in this case.

A striking result of these simulations, and which differentiates defect production in pure metals from that in Ni_3Al, is the prediction of crowd-ion formation at the end of the RCSs along ⟨110⟩ A planes. For B planes, the usual ⟨100⟩ dumbbell is obtained. The complex crowd-ions found here contain lines of anti-site defects. The crowd-ion is not the lowest energy defect in this structure, but apparently a high energy barrier prevents direct conversion into a dumbbell. This behavior is not seen for ⟨110⟩ RCSs on B planes. We performed an annealing at 600 K on one of the crowd-ion configurations to check whether it recovers by one-dimensional migration along the anti-site defect trail to its vacancy, or by converting into a dumbbell and then migrating 3-dimensionally. At that temperature, the defect converted into a dumbbell in less than 1 ps and without migration.

TABLE II. Results of the dynamic simulations of low energy collision events.

PKA	Direction	Energy (eV)	Type of defect	RCS
Al	$\langle 110\rangle^{i}$ (A)	50	Crowd-ion	15
Ni	$\langle 110\rangle^{i}$ (A)	50	Crowd-ion	15
Al	$\langle 110\rangle^{i}$ (A)	30	Crowd-ion	5
Ni	$\langle 110\rangle^{i}$ (A)	30	Crowd-ion	5
Al	$\langle 110\rangle^{i}$ (A)	20	No defect	0
Ni	$\langle 110\rangle^{i}$ (A)	20	No defect	0
Ni	$\langle 110\rangle^{o}$ (A)	35	No defect	0
Ni	$\langle 110\rangle^{o}$ (A)	50	Crowd-ion	13
Ni	$\langle 110\rangle^{o}$ (B)	20	No defect	0
Ni	$\langle 110\rangle^{o}$ (B)	25	No defect	0
Ni	$\langle 110\rangle^{o}$ (B)	30	Dumbbell Ni–Ni (B)	6
Al	$\langle 100\rangle^{o}$ (A)	50	Octahedral Al (B)	1
Ni	$\langle 100\rangle^{o}$ (B)	50	Dumbbell Ni–Ni (B)	3
Ni	$\langle 100\rangle^{o}$ (A)	50	Crowd-ion Ni (A)	2
Al	$\langle 111\rangle^{o}$	200	Octahedral Al (B)	1
Al	$\langle 111\rangle^{o}$	100	No defect	0
Ni	$\langle 111\rangle^{o}$	50	2-ring exchange (2 anti-site defects)	0

First column indicates the PKA. Second column shows the direction of the PKA. These are always a few degrees off the crystallographic directions. "i" and "o" indicate if this direction is contained in the $z = 0$ plane (i), or not (o). Types of defects and number of replacements along a RCS are also indicated.

We have also simulated displacements along the three nonequivalent ⟨100⟩ chains at 50 eV. The result for Al as the PKA is a vacancy at the PKA site, a perfect replacement in the Al site located at $(1,0,0)a_0$, and an octahedral Al interstitial in $(\frac{3}{2},\frac{1}{2},\frac{1}{2})a_0$. The octahedral defect, Al (B), with enthalpy 4.54 eV, is energetically favored over all other Al interstitial positions in an A plane. However, in the perfect lattice, the enthalpy of this configuration is 0.09 eV higher than that of Ni–Al* (B) (see Table I). Whether a barrier prevents this conversion, or whether its interaction with its own vacancy (which is located between the 5th and 6th neighboring shell) inverts the relative enthalpies, has not yet been determined. The close proximity of interstitial and vacancy, however, illustrates that spontaneous recombination volumes in Ni_3Al can be much smaller than in pure metals.

For Ni as the PKA in a ⟨100⟩ event in the A plane, the extra Ni atom adopts the proper crowd-ion Ni (A) configuration with 5.14 eV, instead of the dumbbell Ni–Ni (A) with 4.67 eV. This again can be due either to an interaction with the vacancy or a barrier to rotation. The Ni ⟨100⟩ PKA event in the B plane shows normal behavior, three replacements terminating with a ⟨100⟩ (B) dumbbell.

The ⟨111⟩ direction is extremely hard for defect production in Ni_3Al, perhaps even harder than for pure fcc metals. The threshold energy for events along Al chains is found between 100 and 200 eV with one replacement along the cube diagonal and an octahedral Al (B) interstitial. For the ⟨111⟩ containing Ni atoms, a 50 eV event produced a two-ring exchange with the production of two anti-site defects; i.e., the PKA Ni acquired a nn Al site and this Al atom took the original PKA Ni site; no Frenkel pairs, however, were produced.

III. CONCLUSIONS

The results of these initial studies of defect production and defect properties in Ni_3Al help to elucidate radiation effects in intermetallic compounds. We first note that defect production in Ni_3Al has distinct differences from that in pure fcc metals. First, the crowd-ion, rather than the ⟨100⟩ dumbbell, is produced in low energy events along some ⟨110⟩ events. Moreover, other

configurations of interstitials also seem possible. Until the entire threshold surface is mapped out, however, the relative fraction of each of the configurations in an irradiation experiment cannot be predicted. The simulations also show that the spontaneous recombination volume for some defect configurations in this structure can be much smaller than in pure metals. This may have important implications for radiation-induced amorphization of intermetallic compounds, since each Frenkel pair makes a large contribution to the total enthalpy of the crystalline phase. Lastly, we note that the mass mismatch in the ⟨110⟩ direction (A planes) has only minor influence, if any, on the length of RCS chains, although the plane containing the ⟨110⟩ replacement chain does influence the defect configuration at the end of the chain.

The current simulations of defect enthalpies, together with those for vacancies reported by Foiles, provide a reasonable explanation for the lack of segregation in Ni_3Al. It was shown that the interstitial with lowest enthalpy is the Ni–Ni (B) dumbbell and that other possibilities would energetically convert to this defect even when it requires the creation of an anti-site defect. Since the Ni–Ni (B) interstitial can migrate on the Ni sublattice in three dimensions, it is the only mobile interstitial atom. Similarly, a vacancy can migrate on the Ni sublattice whereas a vacancy on the Al sublattice must switch sublattices and create anti-site defects, which is energetically unfavorable. Thus, most defect motion is restricted to Ni–Ni dumbbells and vacancies migrating on the Ni sublattice. This constrained motion of defects cannot lead to segregation.

ACKNOWLEDGMENTS

The authors are grateful to Dr. M. S. Daw, Dr. S. M. Foiles, and Dr. J. Adams for making the DYNAMO code and Ni–Al data files available to us and for helping to bring them on-line in Switzerland. One of us (RSA) is grateful to his co-authors and the Pirex group for their kind hospitality and stimulating discussions during his stay at the Paul Scherrer Institute. The work was supported, in part, by the United States Department of Energy, Basic Energy Sciences under contract DE-AC02-76ER01198 and the Swiss National Research Foundation.

REFERENCES

[1]J. B. Gibson, A. N. Goland, M. Milgram, and G. H. Vineyard, Phys. Rev. **120**, 1229 (1960).
[2]T. Diaz de la Rubia, R. S. Averback, R. Benedek, and W. E. King, Phys. Rev. Lett. **59**, 1930 (1987).
[3]See, e.g., *Interatomic Potentials and Simulation of Lattice Defects*, edited by P. C. Gehlen, J. R. Beeler, Jr., and R. I. Jaffee (Plenum, New York, 1972).
[4]S. M. Foiles, M. I. Baskes, and M. S. Daw, Phys. Rev. B **33**, 7983 (1986).
[5]G. H. Vineyard, J. Phys. Soc. Jpn. **18**, Suppl. III, 144 (1963).
[6]S. M. Foiles and M. S. Daw, J. Mater. Res. **2** (1), 5 (1987).
[7]T. Bui, J. L. Klatt, I. M. Robertson, and R. S. Averback (unpublished research).
[8]D. I. Potter and D. G. Ryding, J. Nucl. Mater. **71**, 14 (1977).
[9]The DYN52 code was written by M. I. Baskes, M. S. Daw, and S. M. Foiles.
[10]Although the threshold energies have not been determined for Ni_3Al, the values obtained by simulations are typical of those in Ni and other fcc metals. (See, e.g., P. Lucasson, in *Fundamental Aspects of Radiation Damage in Metals,* edited by M.T. Robinson and F.W. Young, Jr. (1975), p. 42.